the material. When we reach SmS, the state immediately above the Fermi energy contains more *f* character than *s*–*d* character, and the lowest-energy state has this electron participating in the occupied *f* subshell; that is, the divalent phase is favoured. This behaviour occurs in the light rare earths, from CeS to EuS, and is repeated in the heavy rare earths from GdS to YbS.

As we go from EuS to GdS in the trivalent state, there is a sudden change in the electronic structure. In trivalent EuS there is a sub-band of six occupied localized spin-up *f* states, plus one spin-up band state which is predominantly *f*-like and which is tied to the Fermi level. The unoccupied *f* bands are held well above the Fermi level by the magnetic splitting. When we go to the trivalent form of GdS, the seventh spin-up *f* band is localized and is no longer tied to the Fermi energy. The spin-up bands then fall closer to the nucleus, to the position they would occupy in the atom. The unoccupied *f* bands can then drop close to the Fermi energy.

There are two rather different types of *f* electron in these materials. The fully occupied *f* states are strongly localized and have the characteristics of core states. These determine the 'valence'. The outer electron is less well localized, meaning that the number of *f* electrons in these materials is not an integer. The difference in the total number of *f* electrons between the divalent and trivalent states changes with atomic number and compound. Hence the traditional view that the number of *f* electrons determines the valence is shown to be not well founded. Consequently, a valence transition is not, in general, a transition between two states with integer numbers of *f* electrons. Rather, it is a transition between two states with integer numbers of localized *f* electrons and an unspecified number of other *f* electrons.

Our discussion of valency implies that there is a direct relationship between the difference in the number of the less well localized *f* electrons and the difference in energy between the two valence states. This is plotted in Fig. 4: a linear relationship is indeed observed. □

1. Jensen, J. & Mackintosh, A.R. *Rare Earth Magnetism* (Oxford Science Publications, Oxford, 1991).
2. Skriver, H. in *Systematics and Properties of the Lanthanides* (ed. Sinha, S.P.) 213–254 (Reidel, Dordrecht, 1983).
3. Johansson, B. Energy position of 4f levels in rare earth metals. *Phys. Rev. B* **20**, 1315–1327 (1979).
4. Delin, A., Fast, L., Johansson, B., Wills, J.M. & Eriksson, O. Method for calculating valence stability of lanthanide systems. *Phys. Rev. Lett.* **79**, 4637–4640 (1997).
5. Svane, A. & Gunnarsson, O. Transition-metal oxides in the self-interaction-corrected density-functional formalism. *Phys. Rev. Lett.* **65**, 1148–1151 (1990).
6. Temmerman, W.M., Svane, A., Szotek, Z. & Winter, H. in *Electronic Density Functional Theory: Recent Progress and New Directions* (eds Dobson, J.F., Vignale, G. & Das M.P.) 327–347 (Plenum, New York, 1998).
7. Jayaraman A. in *Handbook of the Physics and Chemistry of Rare Earths* Vol. 2 (eds Gschneider, K.A. Jr & Eyring, L.R.) 575–611 (North Holland, Amsterdam, 1979).
8. Syassen, K. Ionic monochalcogenides under pressure. *Physica B* **139 & 140**, 277–283 (1986).
9. Syassen, K., Winzen, H., Zimmer, H.G., Tups, H. & Leger, J. M. Optical response of YbS and YbO at high pressure and the pressure-volume relation for YbS. *Phys. Rev. B* **32**, 8246–8252 (1985).

The electronic structure at the atomic scale of ultrathin gate oxides

D. A. Muller, T. Sorsch, S. Moccio, F. H. Baumann, K. Evans-Lutterodt & G. Timp

Bell Laboratories, Lucent Technologies, Murray Hill, New Jersey 07974, USA

The narrowest feature on present-day integrated circuits is the gate oxide—the thin dielectric layer that forms the basis of field-effect device structures. Silicon dioxide is the dielectric of choice and, if present miniaturization trends continue, the projected oxide thickness by 2012 will be less than one nanometre, or about five silicon atoms across[1]. At least two of those five atoms will be at the silicon–oxide interfaces, and so will have very different electrical and optical properties from the desired bulk oxide, while constituting a significant fraction of the dielectric layer. Here we use electron-energy-loss spectroscopy in a scanning transmission electron microscope to measure the chemical composition and electronic structure, at the atomic scale, across gate oxides as thin as one nanometre. We are able to resolve the interfacial states that result from the spillover of the silicon conduction-band wavefunctions into the oxide. The spatial extent of these states places a fundamental limit of 0.7 nm (four silicon atoms across) on the thinnest usable silicon dioxide gate dielectric. And for present-day oxide growth techniques, interface roughness will raise this limit to 1.2 nm.

It is now technologically possible to produce metal oxide semiconductor field effect transistors (MOSFETs) with gates shorter than 50 nm and SiO_2 gate oxides less than 1.3 nm thick[2]. Such a thin gate oxide is required to improve the drain-current response of the transistor to the applied gate voltage (allowing lower voltages to be used). As power dissipation at present limits the scale of integration, lowering the power supply voltage becomes the key to increasing integration and improving integrated-circuit performance. The performance of the gate oxide therefore becomes the limiting factor when manufacturing very-large-scale integrated circuits. As a practical alternative to SiO_2 (or its nitrogenated derivatives), providing a higher dielectric constant or a reduced leakage current, has not been identified yet[1], it is crucial to the future of very-large-scale integration (VLSI) to discover the practical limits on the thickness of the SiO_2 gate oxide.

There are two fundamental considerations. First, the roughness of the interface must be controlled at an atomic scale if such thin oxides are to prove practical. The leakage current through a 1-nm-thick oxide increases by about a factor of 10 for every 0.1-nm increase in the root-mean-square roughness. This leakage current, in conjunction with the subthreshold leakage, is the most important figure of merit in a MOSFET. Second, a single layer of silicon and oxygen has the incorrect topology to reproduce the local electronic structure of bulk silicon dioxide[3]. The question is then how thick must a silicon dioxide layer be before its bulk electrical properties can be obtained? The presence of an intrinsic transition region (which may be a substoichiometric oxide—the 'suboxide') between bulk Si and the bulk-like SiO_2 will place a fundamental limit on drive current by limiting the minimum thickness. Attempts to measure the width of the transition region have given answers that range from structurally abrupt (for molecular beam epitaxy on an atomically flat substrate[4]) to a chemical thickness of 0.3–0.5 nm (for thermally grown[5] oxides). A comprehensive review of earlier work in the field (and the consequences for electronic properties of the interface) is given in ref. 6. However, there is considerable disagreement as to the precise structure and chemical composition of this suboxide[7,8].

Even if the interface structure were known, the connection between the physical arrangement of atoms at the interface and their electrical properties is neither direct nor obvious. Here we focus on measuring the electronic states that directly determine the electrical properties of the interface, which we do with atomic-scale electron-energy-loss spectroscopy (EELS)[9–12]. We use EELS to map the unoccupied electronic density of states by site, atom-column and atomic species. These measurements give localized information about both chemical composition and electronic properties. The work of Batson[11] is particularly relevant for the present study as he demonstrated that a usable Si L edge EELS signal can be obtained from an atomic-sized probe at a Si/SiO_2 interface. To improve the contrast and sensitivity, we found it necessary to use the higher-energy (but weaker) oxygen K edge which is more localized than the Si L edge[13].

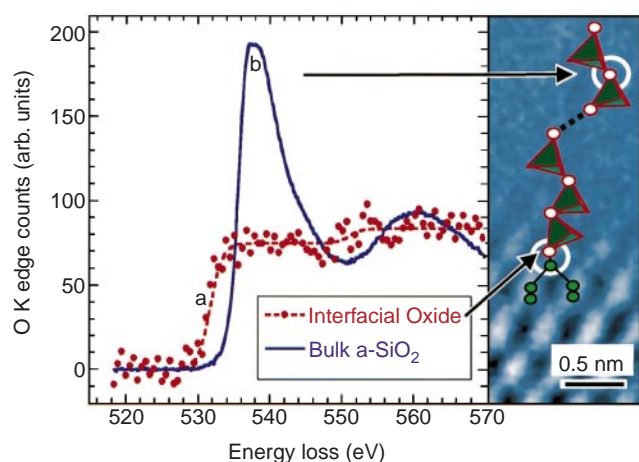The O K and Si $L_{2,3}$ EELS edges provide information on the

Figure 1 The measured EELS O K edges of bulk a-SiO$_2$ and for O atoms at an atomically smooth interface between [100]Si and native a-SiO$_2$. The 3-eV reduction in the edge onset at the interface aligns the unoccupied O interfacial states with the Si conduction band edge, as would be expected for induced gap states. This pre-peak (a) can be thought of as tunnelling states leaking in from the bulk Si. The reduction in the first bulk peak (b) is discussed in the text. The figure to the right is the annular dark field (ADF) image of the interface between the a-SiO$_2$ and the silicon substrate. The image is a projection of the ~100 atoms in the path of the beam, so no structural information can be obtained from the amorphous region where the atoms are not aligned along the beam direction. At a rough interface, the bulk lattice would gradually fade into the background over many lattice spacings. The measurements were performed on the Cornell VG-HB501 100 kV STEM equipped with a cold field-emission gun and a McMullan-style parallel EELS spectrometer. The microscope has been modified to achieve high energy-drift stability (<0.2 eV min^{-1}) and spatial-drift stability (<0.05 nm min^{-1}).

unoccupied O-p, and Si-s,d electronic densities of states (DOS) respectively[14]. The effect of the 2p core hole on the Si L edge is significant, producing a strong exciton. However, the 1s core hole on the O K edge does not introduce any new features at the 1-eV energy resolution used in this study (as we verified by comparison of *ab initio* calculations of the ground-state DOS to the EELS spectra (J. Neaton and D.A.M., unpublished results). This allows a single-particle interpretation of the EELS spectra, which are proportional to local densities of states partitioned in three ways: by site (as the incident probe is localized); chemical species (as each element has unique core level binding energies); and angular momentum (from the dipole selection rules)[15,16]. In a scanning transmission electron microscope (STEM), the EELS measurements are made at internal interfaces, not free surfaces, by passing the 100-keV electron beam (0.2–0.5 nm diameter) through a thin film[9–12,17]. The film is chosen to be thick enough that surface states produce a negligible fraction of the transmitted signal, but also thin enough that multiple scattering is not significant. The interface is oriented parallel to the beam, so that a column of atoms in the interface plane can be measured separately from any atoms in adjacent columns. But because the interface is viewed in projection, any interfacial roughness (especially on length scales thinner than the sample) can lead to an apparent broadening of the interface. We therefore also use X-ray reflectivity to obtain independent measurements of the interface roughness.

We found that the thermal processing needed to grow the gate oxides roughened the interfaces (possibly by microfaceting as the step density is not altered). Consequently, we also searched for a model system containing atomically abrupt interfaces, before examining the thermal oxides. Native oxides which were formed in a dry atmosphere on epitaxial silicon layers produced by chemical vapour deposition (CVD) on [001] silicon could be less than 0.8 nm

thick and have very smooth Si/SiO$_2$ interfaces. The native oxides were prepared for microscopy by adding a protective overlayer of amorphous silicon (a-Si), resulting in Si/SiO$_2$/a-Si sandwich. The O K edge recorded at these smooth interfaces is strikingly different from that for bulk SiO$_2$ (Fig. 1). First, the edge onset (a in Fig. 1) is reduced by 3 eV at the interface with respect to the bulk. As the O K edge reflects the portion of the conduction band projected onto the probed O atom, the reduced edge onset implies a reduced bandgap (which will probably increase the local dielectric constant and electrical conductivity[6]). Second, the sharp peak (b in Fig. 1), which is the first extended-fine-structure peak in the bulk near-edge spectrum, is absent at the interface. X-ray absorption studies of the O K edge in quartz, crystobalite and coesite (three different forms of SiO$_2$ which have the same nearest-neighbour topologies and O–Si–O bond angles but differ mainly in the Si–O–Si bond angles and dihedral angles) all show the same near-edge structure[18]. The same edge shape is also present in GeO$_2$ for the quartz structure, but not for rutile, suggesting that it is the position of the O atoms and not the cations that determines the shape of peak b. Generally, the sharp peak b is identified as arising from O–O scattering and it decreases in intensity as the number of O second-nearest neighbours around the excited O atom are reduced[19]. Essentially, silicon is a much weaker scatterer than O and does not produce strong extended-fine-structure oscillations. We expect a reduction in this peak's intensity even for an atomically abrupt interface as the last layer of O atoms would always lose half its O second-nearest neighbours. (A similar effect can be seen at Cu/MgO interfaces[17]). However, the almost complete absence of this peak implies that more O second-nearest neighbours are missing—that is, the last atom is in a silicon-rich environment. We will use this feature later to estimate the width of the suboxide in the thermally grown gate oxides.

A similar interfacial spectrum is observed at the interface between Si and the thermally grown oxides. Figure 2 shows EELS spectra recorded point by point across a gate stack whose oxide thickness was nominally measured at 1 nm by ellipsometry. The spectrum from each point was decomposed into a linear combination of the bulk and interface signals from Fig. 1, and this decomposition was used to identify the localized relative fractions of bulk-like and interfacial oxide signals (plotted in Fig. 3a). We note that $60 \pm 6\%$ of the total oxygen signal is generated by the interfacial atoms (whose local electronic structure is very different from the bulk). From X-ray reflectivity measurements, we find that the substrate/oxide interface roughness has a standard deviation of $\sigma_r = 0.1$ nm over length scales from 0.1 to 1,000 nm. The projected peak–peak roughness (that is, the distance from minimum to maximum excursion of the silicon substrate) expected in the EELS measurements is then $6\sigma_r = 0.6$ nm. Such roughness will spread out the interfacial signal, such as that in Fig. 3a, without changing its total area. Consequently, the apparent broadness of the lower interface is dominated by the expected 0.6-nm interface roughness, plus the chemical width of the interface (and the 0.27-nm-wide probe added in quadrature). The width of the upper interface between the oxide and the a-Si is half that of the lower interface, but the interfacial areas are the same. This suggests that the main difference between the thermally grown lower interface and the upper interface produced by CVD of a-Si is that the upper interface is much smoother.

The gate stack was then annealed at 1,050 °C for 10 s—a thermal budget typical of that used in device processing. Figure 3b shows that after annealing, the upper interface (which has now been converted to polycrystalline silicon) becomes as rough as the lower. However, the fraction of interfacial signal is essentially unchanged at $50 \pm 5\%$. The most significant difference is that the two interfacial regions now overlap. As the interfacial signal (feature a of Fig. 1) is associated with tunnelling states (discussed below), a large leakage current is expected and observed. This leakage current

759

of 10 A cm^{-2} is higher than desirable for use in integrated circuits[1], but the device is still able to function as a transistor[2], producing drive currents in excess of 1 mA per μm. By increasing the gate oxide thickness to a point where the two interfacial regions no longer overlap, the tunnelling can be reduced. Figure 3c shows a thicker gate oxide (1.8 nm ellipsometric thickness) where the measured electrical-leakage current has been suppressed by 6–7 orders of magnitude. The width of the interface region is not increased in the thicker oxide.

We now estimate the width of the suboxide (that is, the region of substoichiometric oxide) from the line profile of the interface states by recalling that the extended fine structure on the O K edge (especially peak b) is sensitive to the number of second-nearest neighbours that are O atoms[19]. We need to correct for both the interfacial roughness and the fact that the EELS signal is sensitive to second-nearest neighbours as well as nearest neighbours (unlike X-ray photoelectron spectroscopy, XPS). The roughness (and finite instrument resolution) can be accounted for by using the full-width at half-maximum (FWHM) of the total oxygen line-scan (Fig. 3) as a measure of the spatial width of the oxide.

The FWHM of the line profile is independent of interfacial roughness and instrumental spatial resolution, provided that the roughness profile is symmetric about the centre of each interface (as is the case in Fig. 3). For Fig. 3b, the FWHM of the bulk-like oxide is 0.85 ± 0.05 nm. From the ratio of areas of interface and bulk-like

oxide, each interfacial region (defined as that region lacking peak b on the O K edge and hence having fewer oxygen second-nearest neighbours) has a FWHM of 0.43 ± 0.05 nm. The interface thus defined can never be sharper than 0.27 nm (as this is the distance between O second-nearest neighbours, and the last O atom in contact with the bulk Si will always be missing some second-nearest neighbours even at a perfect interface). Consequently, the suboxide cannot be thicker than 0.43–0.27 = 0.16 nm (that is, 1–2 monolayers thick). This upper limit placed by the EELs measurements is consistent with the suboxide thickness inferred indirectly from XPS[5].

The additional electronic states at the interface (feature a in Fig. 1) which appear at energies below the bulk SiO$_2$ conduction band edge are roughly aligned with the bulk silicon conduction band. We identify these as induced gap states[20] resulting from the exponential decay of the silicon conduction band wavefunctions into the oxide (consequently there will be no states in the bandgap of bulk silicon). These evanescent states should be a general feature of any Si/SiO$_2$ interface and should not be very sensitive to the detailed atomic structure. The additional states in the SiO$_2$ bandgap near the interface also imply an altered dielectric constant there. The
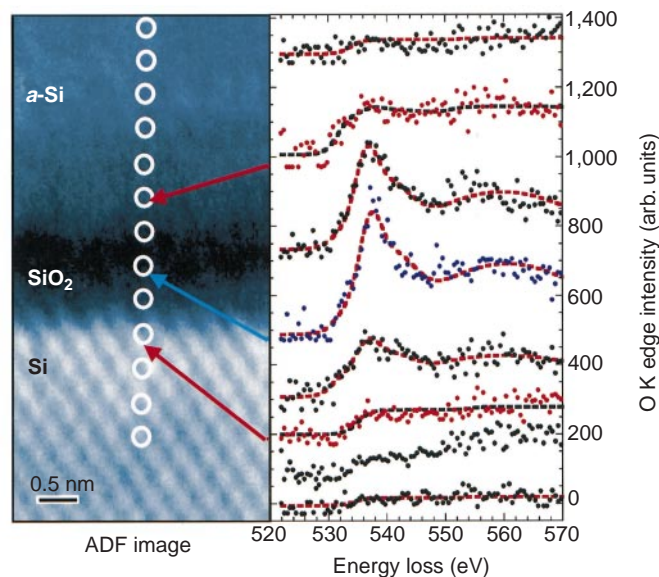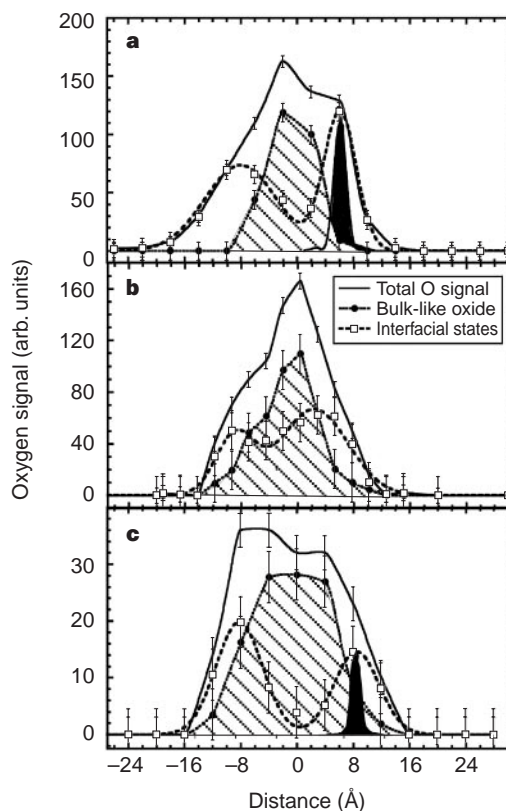

Figure 2 EELS spectra recorded point by point across a gate stack containing a thin gate oxide. The annular dark field (ADF) image (left panel) shows where each spectrum was taken. The [100] silicon substrate is in the lower half, the gate oxide in the middle and the deposited a-Si layer is in top half. The right panel shows the background-corrected O K edges. The smooth curves are the best fits using a mixture of the bulk and interfacial spectra from Fig. 1. The spectra were recorded with a 4-s exposure per point to ensure that the dose was less than the threshold for detectable radiation damage. In growing the gate stacks, particular care was taken to select (using scanning tunnelling microscopy) silicon wafers with exceptionally smooth surfaces before oxidation. The [001]-oriented wafers were cleaned for 15 s in a 15:1 HF solution followed by a 30 s UV-CL clean. The gate oxide was produced by rapid thermal oxidation at 1,000 °C. Chemical vapour deposition (CVD) of a-Si at 550 °C on top of the gate oxide was used as the base of the gate stack, which was subsequently annealed and implanted with dopants. For microscopy, cross-sectioned specimens were dimpled and then ion-milled to electron transparency. The EELS spectra were recorded simultaneously with the ADF signal, under conditions optimized for atomic-resolution imaging[9–12,17]. For a 10-nm-thick sample, the ADF resolution is 0.23 nm and the EELS spatial resolution at the O K edge is reduced to 0.26 nm due to delocalization[13].

Figure 3 Oxygen bonding profiles from O K edge EELS. The substrate is on the left, and the gate contact is on the right: **a**, for a c-Si/SiO$_2$/a-Si stack before annealing (c-Si indicates crystalline Si). The nominal ellipsometric thickness measured after oxidation was 1 nm. From EELS, the total O signal has a FWHM of 1.6 nm and the bulk-like oxide (hatched area) has a FWHM of 0.85 nm. **b**, After annealing for 10 s at 1,050 °C, the a-Si is converted to polycrystalline silicon, roughening the upper interface. The total O signal has a FWHM of 1.3 nm and the bulk-like oxide has a FWHM of 0.85 nm. Although the amount of interfacial oxide has not increased, the increased roughness has resulted in an overlap of the two interfacial regions, almost shorting-out the gate oxide (the leakage current is 10 A cm^{-2}). **c**, In a slightly thicker gate oxide (1.8 nm ellipsometric thickness), the two interfacial signals no longer overlap and the leakage current is reduced to 10^{-5} A cm^{-2}. The total O signal has a FWHM of 2.1 nm and the bulk-like oxide has a FWHM of 1.6 nm. The inelastic point-spread function, which gives a measure of the probe resolution, is shown as black in **a** and **c**.

interfacial dielectric constant will probably be between that of Si and SiO$_2$. The altered dielectric layers are not accounted for in our ellipsometric measurements, in which we assume that the oxide has only the dielectric constant of bulk SiO$_2$. This is probably why ellipsometry has underestimated the width of the oxides in Fig. 3.

The probe localization is obtained by constructing a wavepacket with a transverse momentum spread of more than a reciprocal lattice vector, and consequently all electronic momentum information is lost (as required by the uncertainty principle). Therefore these evanescent states responsible for tunnelling through the oxide and the states from the extended conduction band are treated on an equal footing, and cannot be separated in such a local measurement. In the simplest model, the silicon wavefunctions decay exponentially into the oxide barrier with a decay length for the evanescent states, $\lambda(E)$, determined by the energy difference between the interfacial state (E) and the conduction band edge of bulk SiO$_2$, (E_c), as $\lambda(E) = \hbar/\sqrt{(E_c - E)}$. The tunnelling current depends on the overlap of the evanescent states from either interface. A satisfactory tunnelling barrier is formed when the oxide thickness t is 6λ. This sets an absolute minimum thickness of $t_{min} = 0.7$ nm for an ideal SiO$_2$ gate oxide. Interfacial roughness adds another 6σ_r to t_{min}. The smallest roughness for our thermally grown oxides was 6$\sigma_r = 0.6$ nm which puts a lower limit of 1.2 nm on the practical SiO$_2$ gate oxide thickness. The induced gap states also place severe constraints on the minimum allowed thickness for alternative dielectrics, many of which have large dielectric constants, but reduced bandgaps and hence longer decay lengths. Furthermore, there is the possibility of a reaction between the dielectric and the silicon substrate to form a silicon oxide interlayer. If the interlayer thickness exceeds 1.3 nm (and a typical native oxide is 2 nm thick), the gate capacitance is less than what could be obtained with a pure SiO$_2$ gate oxide. □

1. Semiconductor Industry Association *The National Technology Roadmap for Semiconductors* 71–81 (Sematech, Austin, 1997).
2. Timp, G. *et al.* in *IEDM Technical Digest* 615–618 (IEDM, San Francisco, 1998).
3. Cryot-Lackmann, F. Sur le calcul de la cohesion et de la tension superficielle des mataux de transition par une methode de liasions fortes. *J. Phys. Chem. Solids* **29**, 1235–1243 (1968).
4. Ourmazd, A., Taylor, D. W., Rentschler, J. A. & Bevk, J. Si to SiO$_2$ transformation: interfacial structure and mechanism. *Phys. Rev. Lett.* **59**, 213–216 (1987).
5. Himpsel, F., McFeely, F. R., Taleb-Ibrahimi, A., Yarmoff, J. A. & Hollinger, G. Microscopic structure of the SiO$_2$/Si interface. *Phys. Rev. B* **38**, 6084–6096 (1988).
6. Grunthaner, F. J. & Grunthaner, P. J. Chemical and electronic structure of the Si/SiO$_2$ interface. *Mater. Sci. Rep.* **1**, 65–160 (1986).
7. Pasquarello, A., Hybertsen, M. S. & Car, R. Theory of Si 2p core-level shifts at the Si(001)-SiO$_2$ interface. *Phys. Rev. B* **53**, 10942–10950 (1996).
8. McFeely, F. R., Zhang, K. Z., Banaszak Holl, M. M., Lee, S. & Bender, J. E. An inquiry concerning the principles of the Si 2p core-level photoemission shift assignments at the Si/SiO$_2$ interface. *J. Vac. Sci. Technol. B* **14**, 2824–2830 (1996).
9. Muller, D. A., Tzou, Y., Raj, R. & Silcox, J. Mapping sp^2 and sp^3 states of carbon at sub-nanometre spatial resolution. *Nature* **366**, 725–727 (1993).
10. Muller, D. A., Subramanian, S., Sass, S. L., Silcox, J. & Batson, P. E. Near atomic scale studies of electronic structure at grain boundaries in Ni$_3$Al. *Phys. Rev. Lett.* **75**, 4744–4747 (1995).
11. Batson, P. E. Simultaneous STEM imaging and electron energy-loss spectroscopy with atomic column sensitivity. *Nature* **366**, 727–728 (1993).
12. Browning, N. D., Chisholm, M. M. & Pennycook, S. J. Atomic-resolution chemical analysis using a scanning transmission electron microscope. *Nature* **366**, 143–146 (1993).
13. Muller, D. A. & Silcox, J. Delocalization in inelastic scattering. *Ultramicroscopy* **59**, 195–213 (1995).
14. Egerton, R. F. *Electron Energy Loss Spectroscopy in the Electron Microscope* 2nd edn (Plenum, New York, 1996).
15. Colliex, C. & Jouffrey, B. Diffusion inelastique des electrons dans une solide par excitation de niveaus atomiques profonds. *Phil. Mag.* **25**, 491–514 (1972).
16. Müller, J. E. & Wilkins, J. Band-structure approach to the x-ray spectra of metals. *Phys. Rev. B* **29**, 4331–4348 (1984).
17. Muller, D. A. *et al.* Atomic scale observations of metal-induced gap states at {222} MgO/Cu interfaces. *Phys. Rev. Lett.* **80**, 4741–4744 (1998).
18. Brown, G. E. Jr, Waychunas, G. A., Stohr, J. & Sette, F. Near-edge structure of oxygen in inorganic oxides: effect of local geometry and cation type. *J. Phys.* **47**, (Colloque C8) 685–689 (1986).
19. Wallis, D., Gaskell, P. H. & Brydson, R. Oxygen K near-edge spectra of amorphous silicon suboxides. *J. Microsc.* **180**, 307–312 (1993).
20. Zangwill, A. *Physics at Surfaces* (Cambridge Univ. Press, New York, 1988).

Molecular mechanistic origin of the toughness of natural adhesives, fibres and composites

Bettye L. Smith*†, Tilman E. Schäffer‡†, Mario Viani*, James B. Thompson*, Neil A. Frederick*, Johannes Kindt*, Angela Belcher§, Galen D. Stucky∥, Daniel E. Morse¶ & Paul K. Hansma*

* *Department of Physics,* ∥ *Department of Chemistry and Materials, and* ¶ *Department of Molecular, Cellular, and Developmental Biology, University of California at Santa Barbara, California 93106, USA*
‡ *Department of Molecular Biology, Max-Planck-Institute for Biophysical Chemistry, 37070 Göttingen, Germany*
§ *Department of Chemistry, The University of Texas at Austin, Austin, Texas 78712, USA*
† *These authors contributed equally to this work*

Natural materials are renowned for their strength and toughness[1–5]. Spider dragline silk has a breakage energy per unit weight two orders of magnitude greater than high tensile steel[1,6], and is representative of many other strong natural fibres[3,7,8]. The abalone shell, a composite of calcium carbonate plates sandwiched between organic material, is 3,000 times more fracture resistant than a single crystal of the pure mineral[4,5]. The organic component, comprising just a few per cent of the composite by weight[9], is thought to hold the key to nacre's fracture toughness[10,11]. Ceramics laminated with organic material are more fracture resistant than non-laminated ceramics[11,12], but synthetic materials made of interlocking ceramic tablets bound by a few weight per cent of ordinary adhesives do not have a toughness comparable to nacre[13]. We believe that the key to nacre's fracture resistance resides in the polymer adhesive, and here we reveal the properties of this adhesive by using the atomic force microscope[14] to stretch the organic molecules exposed on the surface of freshly cleaved nacre. The adhesive fibres elongate in a stepwise manner as folded domains or loops are pulled open. The elongation events occur for forces of a few hundred piconewtons, which are smaller than the forces of over a nanonewton required to break the polymer backbone in the threads. We suggest that this 'modular' elongation mechanism might prove to be quite general for conveying toughness to natural fibres and adhesives, and we predict that it might be found also in dragline silk.

We have looked for the mechanism behind the toughness of the organic adhesives and fibres, and, in particular, at the nacre in abalone shells. Analysis of the insoluble organic matrix from the abalone shell revealed a fibrous core in the interlamellar sheets placed between successive nacre tablets[5,15,16], which probably serve as an adhesive holding the tablets together. The organic adhesive is readily apparent when the tablets are pulled apart (Fig. 1). At least one protein, lustrin A, has been isolated from this insoluble organic matrix. The complementary DNA and translated protein sequence reveal that the structure of this protein consists of about 10 alternating and highly conserved cysteine-rich and proline-rich domains, demonstrating that the structure is highly modular[17]. Immuno-histochemical analysis of the fibres (Fig. 1) revealed lustrin A to be a component of the adhesive between the nacre mineral tablets.

Rief *et al.*[18,19] demonstrated that the modular structure of a single molecule can be examined by attaching the molecule between a flat surface and a cantilever of an atomic force microscope (AFM). By pulling on the protein titin and plotting the force versus extension curves, these authors measured the force required to break open the individual subunit in its modular structure. As the titin